



Microbial necromass underpins long-term soil carbon stability and ecosystem carbon persistence in pine reforestations



Shiyang Wu^a, Liehua Tie^{a,b,c,d,*}, Jordi Sardans^{c,d}, Xingliang Xu^e, Ji Chen^f, Peilei Hu^g, Lei Deng^h, Yixian Kong^b, Shengnan Ouyang^a, Congde Huang^{b,i}, Josep Peñuelas^{c,d}, Guijie Ding^a

^a Institute for Forest Resources and Environment of Guizhou, Guizhou Key Laboratory of Forest Cultivation in Plateau Mountain, College of Forestry, Guizhou University, Guiyang 550025, China

^b Forest Ecology and Conservation in the Upper Reaches of the Yangtze River Key Laboratory of Sichuan Province, College of Forestry, Sichuan Agricultural University, Chengdu 611130, China

^c CSIC, Unitat D'Ecologia Global CREA-FCM-UAB, Edifici C, Universitat Autònoma de Barcelona, Bellaterra, Barcelona 08193, Spain

^d CREA, Cerdanyola Del Vallès, Barcelona 08193, Spain

^e Key Laboratory of Land Surface Pattern and Simulation, Key Laboratory of Ecosystem Network Observation and Modeling, Institute of Geographic Sciences and Natural Resources, Chinese Academy of Sciences, Beijing 100101, China

^f State Key Laboratory of Loess and Quaternary Geology, Institute of Earth Environment, Chinese Academy of Sciences, Xi'an 710061, China

^g Institute of Subtropical Agriculture, Chinese Academy of Sciences, Changsha 410125, China

^h State Key Laboratory of Soil and Water Conservation and Desertification Control, Northwest A&F University, Yangling 712100, China

ⁱ Sichuan Mt. Emei Forest Ecosystem National Observation and Research Station, Leshan 614200, China

ARTICLE INFO

Keywords:

Ecosystem carbon storage
Soil Organic Carbon (SOC) fractions
Microbial necromass
Stand age
Pinus massoniana

ABSTRACT

The long-term carbon (C) sequestration potential of plantations hinges on the dynamics and persistence of mature forest C sinks, yet how C storage and stability evolve with increasing forest age remains unclear. Here, we examined a chronosequence of mature *Pinus massoniana* reforestations (32-, 45-, and 60-year-old) to quantify ecosystem C storage across plant (tree, shrub, and herb), litter, and soil (0–100 cm) pools, and to assess soil organic carbon (SOC) stability via the ratio of mineral-associated organic carbon (MAOC) vs. particulate organic carbon (POC). Results showed that the total ecosystem C storage remained relatively constant across stand developmental stages, reflecting that plant C storage increased 53.4% from 32 to 45 years, then declined, while SOC storage decreased 53.9% from 32 to 45 years, then increased. In contrast, the 64.0% rise in the MAOC/POC ratio from 32 to 60 years may reflect a trend of enhanced SOC stability. Microbial necromass constituted 45.9%–64.8% of SOC, with fungal necromass dominating bacterial necromass, especially in the subsoils (20–100 cm). Additionally, SOC, POC, and MAOC showed strong positive correlations with microbial necromass but exhibited weak associations with plant and litter C pools. The MAOC/POC ratio correlated strongly with the ratio of fungal necromass carbon (FNC) vs. bacterial necromass carbon (BNC). These results reveal that microbial—especially fungal—necromass may underpin the soil C stability and ecosystem C persistence of mature pine reforestations. Therefore, accurately predicting the long-term C sequestration of mature reforestation requires a mechanistic understanding that integrates both SOC stability and microbial necromass dynamics.

1. Introduction

Forests are widely recognized as an essential natural solution for mitigating climate change due to their high carbon (C) sequestration capacity, and have been prioritized in numerous national and international initiatives (Griscom et al., 2017; Pugh et al., 2019). Consequently,

plantation forests, particularly through afforestation and reforestation efforts, have expanded at a rate of 2.4% per year, now accounting for 7.4% of the global forest cover (FAO, 2020; Xu et al., 2024). However, the long-term carbon sequestration of these plantations remains uncertain (Shan et al., 2025; Shang et al., 2023; Xu et al., 2024). One key reason is that the forest age strongly regulates the magnitude and timing

* Corresponding author. Institute for Forest Resources and Environment of Guizhou, Guizhou Key Laboratory of Forest Cultivation in Plateau Mountain, College of Forestry, Guizhou University, Guiyang 550025, China.

E-mail address: lhtie@gzu.edu.cn (L. Tie).

Peer review under the responsibility of Editorial Office of Forest Ecosystems.

<https://doi.org/10.1016/j.fecs.2026.100457>

Received 25 November 2025; Received in revised form 5 March 2026; Accepted 5 March 2026

2197-5620/© 2026 The Authors. Publishing services by Elsevier B.V. on behalf of KeAi Communications Co. Ltd. This is an open access article under the CC BY-NC-ND license (<http://creativecommons.org/licenses/by-nc-nd/4.0/>).

of C sequestration (Shan et al., 2025; Shang et al., 2023; Tang et al., 2014). Moreover, the enduring long-term C sequestration of afforestation and reforestation depends not only on C accumulation but also on the persistence of C sinks in mature forests (Bossio et al., 2020; Liu et al., 2025b; Minasny et al., 2017; Zhou et al., 2006). This highlights the need to quantify both the storage and stability of C—two critical parameters in forest C models (Bar-On et al., 2025; Bossio et al., 2020; Liu et al., 2025b)—to better understand when planted forest C sinks occur and our ability to predict their continued future existence.

The multi-compartment storage of C in forest ecosystems, across plant biomass, litter layer, and particularly in soil organic matter, forms the foundational framework for assessing C storage (Bani et al., 2018; Minasny et al., 2017; Pugh et al., 2019). Early-stage stands typically exhibit higher plant growth rates and greater biomass C accumulations (Hua et al., 2022; Justine et al., 2017), whereas mature forests display more complex C dynamics. As forests aging, net primary productivity tends to decline, potentially reducing biomass C accumulation (Shang et al., 2023; Tang et al., 2014). Empirical evidence from Shang et al. (2023) demonstrates that young and intermediate-aged forests exhibit enhanced tree biomass C, whereas forest aging (35–75 years) correlates with an 8%–17% reduction in net primary productivity. These findings suggest that mature forest ecosystems may experience slower biomass C accumulation than younger forests (Justine et al., 2017; Shang et al., 2023). Nevertheless, aging can also enhance understory vegetation diversity, which may stabilize or even increase biomass C storage in old-growth forests (Li et al., 2023; Zhou et al., 2017). Additionally, the global forest litter pool represents a substantial C reservoir, estimated to currently store more than 2,830 Tg of C (Bani et al., 2018). Its net changes with stand age result from the balance between litterfall inputs and decomposition losses (Bani et al., 2018; Prescott, 2010). Many studies report that increasing litter C storage from middle-aged to mature forests followed by stabilization (Güner et al., 2024; Xu et al., 2025). By contrast, soil organic carbon (SOC) storage dynamics with stand aging are less consistent. Although SOC storage often increases with stand development (Li et al., 2023; Zeng et al.), other studies report a decrease (Zhou et al., 2017) or no significant trends (Justine et al., 2017; Zhu et al., 2017).

Beyond C storage capacity, the stability of SOC has emerged as a crucial determinant of long-term C sequestration in forests (Angst et al., 2023; Cotrufo et al., 2019; Lavalley et al., 2019; Liu et al., 2025b). SOC stability is governed by the balance between functionally distinct fractions, namely mineral-associated organic carbon (MAOC, <53 μm) and particulate organic carbon (POC, >53 μm) fractions (Angst et al., 2023; Cotrufo et al., 2019; Lavalley et al., 2019). MAOC stabilized through mineral adsorption and physical protection within soil aggregates, demonstrates remarkable persistence, remaining stable for centuries to millennia (Angst et al., 2023; Lavalley et al., 2019). Conversely, POC primarily comprises partially decomposed plant residues and demonstrates relatively rapid turnover rates (Angst et al., 2023; Lavalley et al., 2019; Witzgall et al., 2021). Therefore, the MAOC/POC ratio serves as a useful indicator of SOC stability (Liu et al., 2025b; Nuralkyzy et al., 2023; Reinsch et al., 2025). However, reported POC and MAOC dynamics with forest aging are inconsistent, showing increases (Su et al., 2023; Zhao et al., 2024), decreases (Zhang et al., 2022b), and negligible changes (Zhang et al., 2022a; Zhao et al., 2024). Importantly, most studies focus on topsoil layers (0–20 cm) (Su et al., 2023; Yost and Hartemink, 2020), even though over 70% of SOC resides below 20 cm (Hicks Pries et al., 2023). Deep soil layers, characterized by reduced root and microbial biomass and enhanced mineral contents, may exhibit different stabilization mechanisms with stand aging (Hicks Pries et al., 2023; Xu et al., 2020). Quantifying SOC stability throughout both topsoil and subsoil profiles is thus essential for a complete understanding of forest C dynamics.

Plants and microorganisms are recognized as the key drivers for the formation and transformation of forest SOC (Feng, 2022; Hu et al., 2023; Kallenbach et al., 2016; Wang et al., 2021). Plant-derived C enters the

soil mainly through litter decomposition and root exudation (Adamczyk et al., 2019a; Feng, 2022; Sokol et al., 2018a), while microbial-derived C originates from microbial turnover and contributes to the formation of persistent microbial necromass carbon (MNC) (Lavalley et al., 2019; Liang et al., 2017; Tao et al., 2023). Amino sugars are reliable biomarkers of MNC, with glucosamine (GluN) and muramic acid (MurA) representing fungal necromass carbon (FNC) and bacterial necromass carbon (BNC), respectively (Joergensen, 2018). Microbial necromass contributes disproportionately to MAOC formation via sorption to clay minerals and Fe/Al (hydr) oxides, thereby promoting long-term SOC stabilization (Angst et al., 2023; Sokol et al., 2018b). Although MNC has recently been recognized as a dominant and stable SOC source globally (Kallenbach et al., 2016; Liang et al., 2017; Wang et al., 2021), its temporal dynamics and relative importance compared to plant-derived inputs across forest development remain poorly understood.

As a native pioneer tree species, *Pinus massoniana* has been extensively utilized in afforestation and reforestation initiatives across subtropical regions of China (Dou et al., 2013; Zhang et al., 2022a). This species plays a crucial role in timber production, C sequestration, and ecosystem services (Bai et al., 2020; Cao et al., 2024; Guo et al., 2023). Research indicates that C accumulation in *P. massoniana* plantations demonstrates distinct stage-dependent patterns, characterized by increasing plant biomass C storage during initial reforestation phases, while soil C pools may either progressively accumulate or maintain relative unchanged (Justine et al., 2017; Xiang et al., 2024). However, existing research has primarily focused on young to near-mature plantations (<30 years) (Dou et al., 2013; Zhang et al., 2022a). The dynamics of ecosystem C storage and SOC stability in mature forests (>30 years) remain poorly understood. Moreover, previous studies have mostly focused on the surface soils (e.g., 0–30 cm) (Guo et al., 2023; He et al., 2021; Shen et al., 2023), overlooking potentially large and age-sensitive C pools in deeper layers (Dubeux et al., 2024; Hicks Pries et al., 2023).

To address these gaps, we investigated mature *P. massoniana* reforestation across three age classes: 32, 45, and 60 years old. We collected samples from plant communities (trees, shrubs, and herbs), litter layer, and soil profiles. Soil sampling extended to 100 cm depth to capture whole-profile organic carbon dynamics. Our study had three specific objectives: (1) To quantify total ecosystem C storage and its partitioning among plant, litter, and soil pools along the chronosequence; (2) to assess SOC stability dynamics in mature forests using the MAOC/POC ratio; and (3) to identify the relationship among soil POC and MAOC dynamics and their drivers (e.g., plant, litter, or microbial necromass) throughout stand development stages. Furthermore, we also aim to enhance the understanding of C persistence in mature reforestation ecosystems. Particular emphasis is placed on older stands and deeper soil layers, two critical yet underexplored dimensions essential for accurately forecasting forest C sinks under sustainable management strategies.

2. Materials and methods

2.1. Study site and experimental design

This study was conducted at the National Long-term Scientific Research Station of Guizhou University, located at 106°45′–107°11′ E and 26°22′–26°45′ N, with an elevation range of 1,250–1,350 m (Fig. S1a). The research site experiences a subtropical humid monsoon climate, characterized by a mean annual temperature of 13.5 °C and mean annual precipitation of 1,200 mm. Large-scale reforestation initiatives have been implemented at the research site since the mid-20th century. Specifically, *P. massoniana* plantations were established in 1963 (60-year-old, 50 ha), 1978 (45-year-old, 100 ha), and 1991 (32-year-old, 80 ha). Prior to *P. massoniana* reforestation, the area was primarily covered by mixed evergreen and deciduous broadleaf forests with approximately 23 g•kg⁻¹ top SOC. The original forest ecosystem, including understory vegetation, was cut down before reforestation

within one year. Since plantation establishment, all stands were thinned at intervals of approximately of eight to ten years to improve stand productivity and promote tree growth. Thinning followed a standardized protocol: operations were initiated when canopy density exceeded 0.9, with removal intensity determined by the target post-thinning density. Canopy density was maintained between 0.6 and 0.7 after each thinning event. All logging residues (e.g., deadwood, branches, and leaves) were subsequently removed from the study plots. The soil, classified as a Ferralsol according to the World Reference Base for Soil Resources (WRB, 2015), consists of old alluvial yellow loam with a depth of approximately 120 cm. Additional details regarding the study site and experimental design are available in Tie et al. (2024).

This study employed a space-for-time substitution approach, investigating mature *P. massoniana* reforestations of three age classes: 32, 45, and 60 years. Between August 15 and 30, 2022, we established fifteen 20 m × 20 m plots, with five replicates per stand age group (Fig. S1b). All plots were separated by a minimum distance of 500 m to ensure spatial independence, with spatial variability quantified. We conducted individual tree measurements for all *P. massoniana* specimens within each plot. Mean diameter at breast height (DBH) values for *P. massoniana* were 34.9 ± 3.9 (60-year-old), 27.6 ± 2.9 (45-year-old), and 20.1 ± 1.0 cm (32-year-old). Stand densities averaged 550 ± 21 (60-year-old), 764 ± 25 (45-year-old), and 1,300 ± 61 stems•ha⁻¹ (32-year-old). Detailed plot characteristics are presented in Table S1.

2.2. Plant and litter sampling and analysis

Plant and litter sampling was carried out across all study plots in August 2022. Three representative trees with average stand-level DBH were selected per plot. From each selected tree, we collected approximately 100 g of mature green leaves and 200 g of branches from the upper canopy for C content and storage analysis. Given the limited root biomass of understory vegetation, sampling focused exclusively on *P. massoniana* roots. Fine root samples (<2 mm diameter) were collected through systematic soil excavation along the root system from base to tip. Approximately 10 g of fine roots per tree were combined into composite samples for C analysis. Stem cores were extracted at breast height from each selected tree using an increment borer. *P. massoniana* biomass components (leaves, branches, stems, and roots) were quantified using an allometric growth model that relates biomass to DBH (Návar, 2009), see below.

Five subplots were systematically established for understory vegetation and litter sampling, positioned at the center and along the diagonals of each main plot (Fig. S1c). Within each 2 m × 2 m shrub subplot, stems and leaves were collected and homogenized into composite samples for biomass quantification and C analysis. Similarly, all herbaceous vegetation within 1 m × 1 m subplots was harvested (Fig. S1c). As leaf litter constitutes approximately 90% of annual litterfall in *P. massoniana* reforestations (Bai et al., 2023), our sampling focused primarily on this component. All leaf litter within 0.5 m × 0.5 m subplots was collected for biomass determination and C analysis (Fig. S1c). Biomass was determined by oven-drying samples at 60 °C to constant weight, followed by precise weighing. Dried samples were ground and sieved through a 0.1 mm mesh for C content analysis, with C storage calculated as the product of biomass and C content.

2.3. Soil sampling and analysis

Five soil sampling subplots were established at the midpoint and along the diagonals of each study plot for soil profile analysis (Fig. S1c and S1d). Soil samples were collected at depths of 0–20, 20–60, and 60–100 cm. Samples were uniformly collected from each depth layer, proceeding from top to bottom, to obtain approximately 1,000 g of soil per layer, which were then thoroughly homogenized to create depth-specific composite samples. In the laboratory, composite samples were manually cleaned of roots and gravel using tweezers. Each processed soil

sample was divided into two subsamples. One subsample was stored at 4 °C for microbial biomass carbon (MBC) analysis, completed within one week of collection. Another subsample was air-dried and sequentially sieved through 2 and 0.149 mm meshes for analysis of SOC, its fractions (POC and MAOC), and amino sugars.

SOC was fractionated into POC and MAOC following the wet sieving and particle size fractionation protocol (Lavalley et al., 2019). For the fractionation process, 10 g of air-dried soil (sieved through 2 mm) was transferred to a 50 mL Erlenmeyer flask. A 5% (w/v) sodium hexametaphosphate solution was added, and the mixture was shaken at 90 r•min⁻¹ for 18 h using an orbital shaker to achieve complete soil dispersion. The dispersed suspension was filtered through a 53 µm sieve, where the <53 µm fraction was collected as MAOC and the >53 µm fraction was retained as POC. Both fractions were oven-dried at 60 °C to constant weight, followed by C content determination using the Walkley-Black potassium dichromate oxidation method (Walkley and Black, 1934).

MBC was quantified using the chloroform fumigation-K₂SO₄ extraction method (Brookes et al., 1985), with C content in the extracts measured by a total organic carbon analyzer (Vario TOC, Elementar, Germany). Soil amino sugar content was analyzed following the hydrochloric acid hydrolysis-gas chromatography protocol (Camenzind et al., 2023). For the analysis, 0.5 g of air-dried soil (sieved through 0.149 mm) was weighed into a hydrolysis flask, followed by the addition of 10 mL of 6 mol•L⁻¹ hydrochloric acid. Following nitrogen purging, samples were hydrolyzed at 105 °C for 8 h. After adding 100 µL of inositol as an internal standard, the hydrolysate was filtered and concentrated to dryness using a rotary evaporator. The necromass was re-dissolved in ultrapure water, and the pH was adjusted to 6.6–6.8 with potassium hydroxide before centrifugation to remove precipitates. The supernatant was dried under nitrogen, re-suspended in methanol, and centrifuged again. Then, the subsample was concentrated and re-dissolved in ultrapure water and lyophilized. Derivatization was performed using acetic anhydride under heating, followed by the addition of hydrochloric acid in dichloromethane. The organic phase was washed with deionized water, dried under a nitrogen stream, and reconstituted in a 1:1 (v/v) ethyl acetate:n-hexane mixture. Amino sugar concentrations, including GlcN and MurA, were quantified by gas chromatography using an UltiMate 3000 system (Agilent, USA).

2.4. Statistical analysis

The biomass of *P. massoniana* leaves, branches, stems, roots, and total tree layer biomass was estimated using an allometric growth model based on the relationship between biomass and DBH (Návar, 2009):

$$W_{l,br,s,r} = a_{l,br,s,r} \times \text{DBH}^{b_{l,br,s,r}} \quad (1)$$

where W indicates the biomass of each organ (kg); l, br, s and r indicate leaf, branch, stem, root, respectively; a is the proportionality constant, representing the initial proportional relationship between tree biomass and DBH; b is the allometric growth exponent, reflecting the nonlinear growth rate of tree biomass as DBH changes, and revealing the strength and morphological characteristics of the relationship between DBH and tree biomass. The values of both parameters vary across different DBH classes and plant organs (Gao et al., 2016).

The content of plant and litter C was determined using the external heating potassium dichromate oxidation method (Walkley and Black, 1934). The storage of plant and litter C was calculated as Eq. 2:

$$\text{C storage} = \text{biomass} \times \text{C content} \times 10^{-6} \quad (2)$$

where C storage is in t•ha⁻¹, biomass is in kg•ha⁻¹, and C content is in g•kg⁻¹.

The bacterial, fungal, and MNC contents were calculated using Eqs. 3–5 (Hu et al., 2024):

$$\text{BNC} = \text{MurA} \times 31.3 \quad (3)$$

$$\text{FNC} = (\text{GlcN} - 1.16 \times \text{MurA}) \times 10.8 \quad (4)$$

$$\text{MNC} = \text{BNC} + \text{FNC} \quad (5)$$

The storage of SOC, POC, MAOC, MBC, and MNC (including BNC and FNC) was calculated as in Eq. 6 (Grimm et al., 2008):

$$\text{Soil C storage} = 0.1 \times \text{C content} \times \text{soil bulk density} \times \text{soil layer depth} \quad (6)$$

where Soil C storage is in $\text{t} \cdot \text{ha}^{-1}$, C content in $\text{g} \cdot \text{kg}^{-1}$, soil bulk density is in $\text{g} \cdot \text{cm}^{-3}$, and soil layer depth is in cm.

Linear mixed-effects models with restricted maximum likelihood (REML) estimation were employed to assess the impact of stand age on C content and storage in plant components (including *P. massoniana* and understory vegetation), litter, and the total ecosystem. In these models, stand age was treated as a fixed effect, while study plot and stand density were included as random effects. Furthermore, linear mixed-effects models with REML estimation were implemented to evaluate the effects of stand age, soil depth, and their interaction on the content and storage of SOC, its fractions (POC and MAOC), MBC, MNC (including BNC and FNC), and the MAOC/POC ratio. In these models, stand age and soil depth were specified as fixed effects, while study plot and stand density were incorporated as random effects. To prevent biased estimates from spatial pseudoreplication and obtain generalizable conclusions, we modeled plot and stand density as random effects in this study. Post hoc multiple comparisons were performed using Tukey's Honestly Significant Difference (HSD) test at a 95% confidence level ($p < 0.05$).

To investigate the temporal dynamics of relationships among plant, litter, and soil C pools across stand developmental stages, Spearman correlation analysis was conducted to evaluate the associations among plant and litter C pools and SOC and its fractions. To examine the temporal dynamics between microbial and soil C pools across stand developmental stages, linear regression analysis was performed to quantify the relationships among MNC (including BNC and FNC) and

SOC, POC, and MAOC contents. To further investigate the relationship between SOC stability and microbial necromass, linear regression analysis was employed to assess the association between the MAOC/POC ratio and the FNC/BNC ratio. All statistical analyses were conducted using R version 4.4.2 (R Core Team, 2024) on Windows platform.

3. Results

3.1. Dynamics of ecosystem carbon storage and its allocation along the chronosequence

Plant (*P. massoniana* and understory vegetation) C storage increased significantly by 53.4% from 32 to 45 years, but decreased slightly by 20.6% from 45 to 60 years (Fig. 1a, b, and e). Litter C storage remained stable across the three stand ages (32, 45, and 60 years), showing no significant variations (Fig. 1c and e). SOC storage in the 0–100 cm profile exhibited a significant reduction of 53.9% from 32 to 45 years (particularly in the 0–60 cm layer), followed by a substantial increase of 68.2% from 45 to 60 years (Fig. 1d and e). Overall, ecosystem C storage showed no significant changes across the three stand ages (Fig. 1e).

3.2. Dynamics of SOC fractions and their stability along the chronosequence

Both the content and storage of soil POC showed significant declines from 32- to 45-year-old stands, with this decreasing trend continuing through to 60-year-old stands (Fig. 2a and c). The content and storage of MAOC exhibited a significant reduction from 32 to 45 years, followed by a modest recovery from 45 to 60 years (Fig. 2b and d). Across the 0–100 cm soil profile, the MAOC/POC ratio demonstrated a consistent upward trend along the chronosequence, reaching significantly higher values in 60-year-old stands compared to 32-year-old stands (particularly in the 60–100 cm soils; Fig. 3). This pattern may at least partly contribute to enhanced SOC stability along the chronosequence.

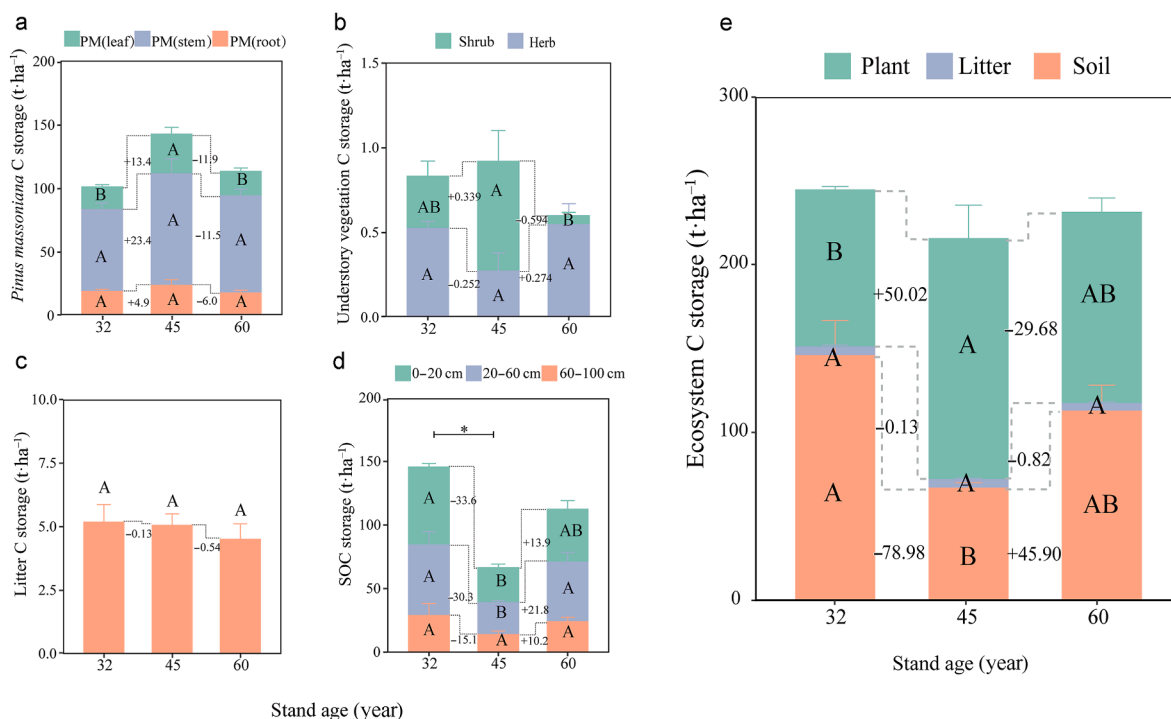


Fig. 1. Dynamics of ecosystem carbon storage (e) and its allocation (a–e) across stand developmental stages. PM (leaf), PM (stem), and PM (root) represent the leaves (including leaves and branches), stems, and roots of *P. massoniana*, respectively. The values are the means \pm standard error of five replicate plots. Different capital letters denote significant differences between stand ages at the same *P. massoniana* organs, understory vegetation types, and soil depth ($p < 0.05$). The horizontal lines compare the differences in total C storage between different stand ages. Significance levels are as follows: * $p < 0.05$.

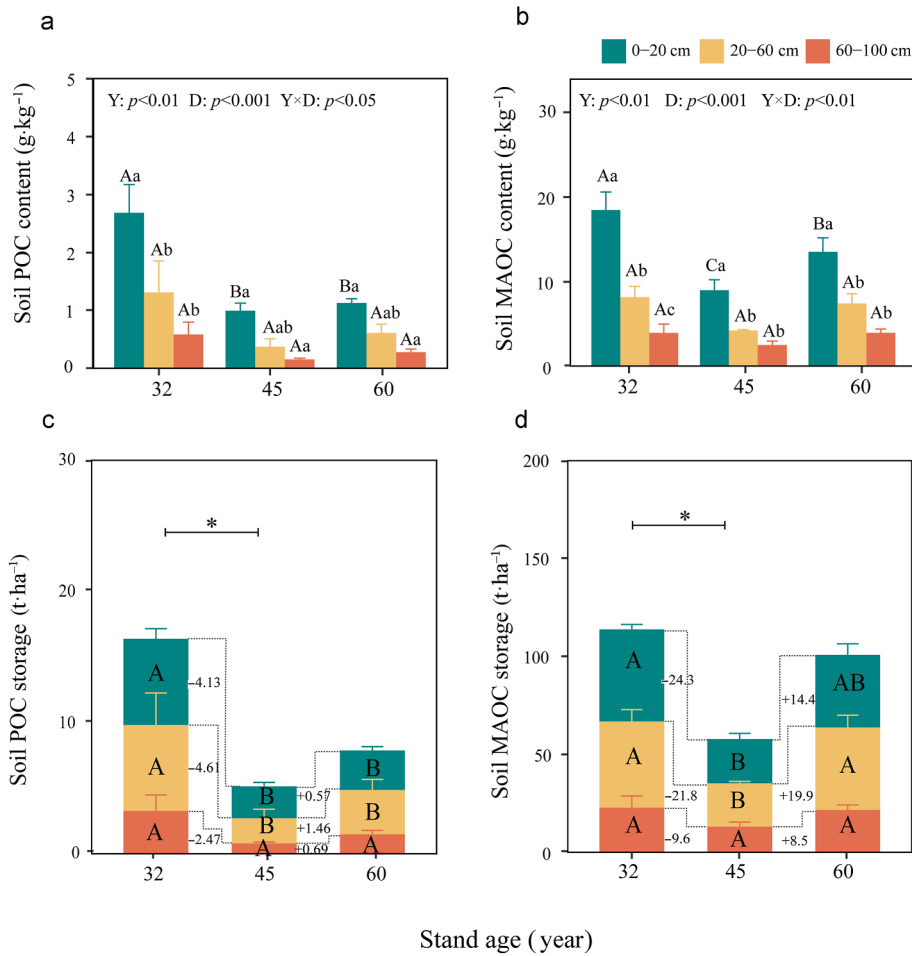


Fig. 2. Dynamics of SOC fractions (a and b) content and (c and d) storage across stand developmental stages. The values are the means ± standard error of five replicate plots. Y, D, and Y × D represent the main effects of stand age, soil depth, and their interactions, respectively. Different capital letters denote significant differences between stand ages at the same soil depth ($p < 0.05$), and different lower-case letters denote significant differences between soil depth at the same stand ages ($p < 0.05$). The horizontal lines compare the differences in total C storage between different stand ages. Significance levels are as follows: * $p < 0.05$.

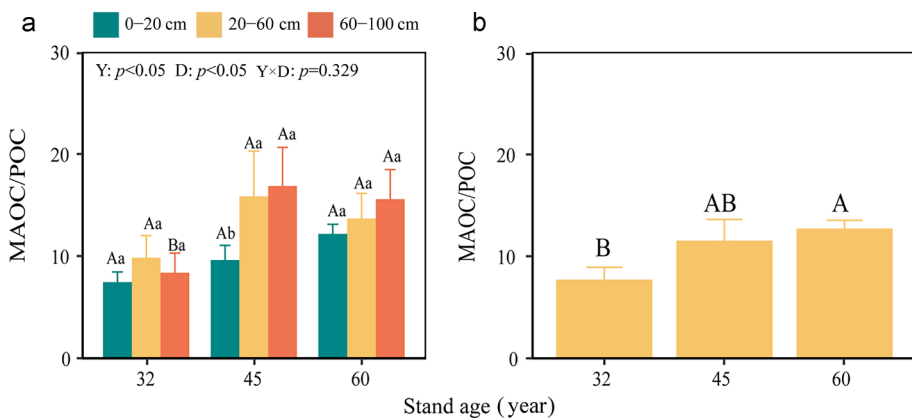


Fig. 3. Dynamics of the MAOC to POC ratio across stand developmental stages. (a) Differences in the MAOC to POC ratio among different stand ages and soil depth. (b) Differences in the 0–100 cm MAOC to POC ratio among different stand ages. The values are the means ± standard error of five replicate plots. Y, D, and Y × D represent the main effects of stand age, soil depth, and their interactions, respectively. Different capital letters denote significant differences between stand ages at the same soil depth ($p < 0.05$), and different lowercase letters denote significant differences between soil depths at the same stand age ($p < 0.05$).

3.3. Dynamics of microbial biomass and necromass carbon along the chronosequence

MBC content and storage in the 0–100 cm soil profile remained stable across the three stand ages, showing no significant variations (Fig. 4a and e). However, in the 0–100 cm layer, the storage of BNC, FNC, and MNC decreased by 55.3%, 52.0%, and 52.8%, respectively,

from 32 to 45 years, and increased from 45 to 60 years (although it was not significant, Fig. 4f–h). The proportion of MNC to SOC did not change significantly along the chronosequence, but it was high (45.9%–64.8% proportion), especially in the 20–100 cm soil layer (always over 50% proportion) (Fig. S3). Additionally, fungal necromass contributions to SOC consistently exceeded those from bacterial necromass in the 20–100 cm layer across the three stand ages (Fig. S3). These results

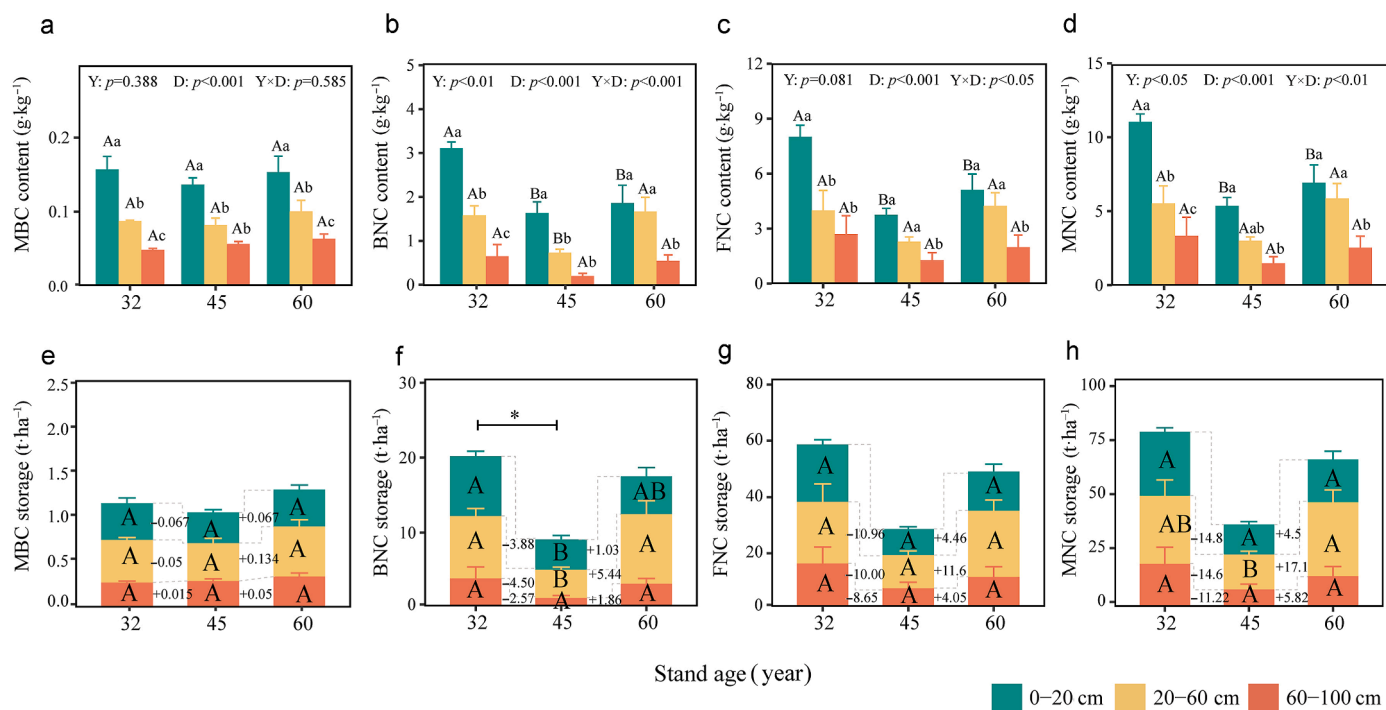


Fig. 4. Dynamics of microbial biomass and necromass carbon (a–d) content and (e–h) storage across stand developmental stages. The values are the means ± standard error of five replicate plots. Y, D, and Y × D represent the main effects of stand age, soil depth, and their interactions, respectively. Different capital letters denote significant differences between stand ages at the same soil depth ($p < 0.05$), and different lowercase letters denote significant differences between soil depths at the same stand age ($p < 0.05$). The horizontal lines compare the differences in ecosystem C storage between different stand ages. Significance levels are as follows: * $p < 0.05$.

indicate that microbial—especially fungal—necromass likely plays a dominant role in contributing to SOC content, particularly in the subsoil.

3.4. Relationships among plant, litter, microorganism, and SOC fractions

Our results highlight that SOC, POC, and MAOC have stronger correlations with MNC (especially fungal necromass) compared to the plant

and litter C pools (Figs. 5 and 6). Specifically, SOC, POC, and MAOC showed individual significant correlations with the parameters of *P. massoniana*, understory vegetation, and litter C storage (Fig. 5). However, a significant positive correlation was found among SOC as well as MAOC contents and MNC, BNC, and FNC across all soil layers (Fig. 6). Notably, a significant positive correlation was found between the MAOC/POC ratio and the FNC/BNC ratio (Fig. S4).

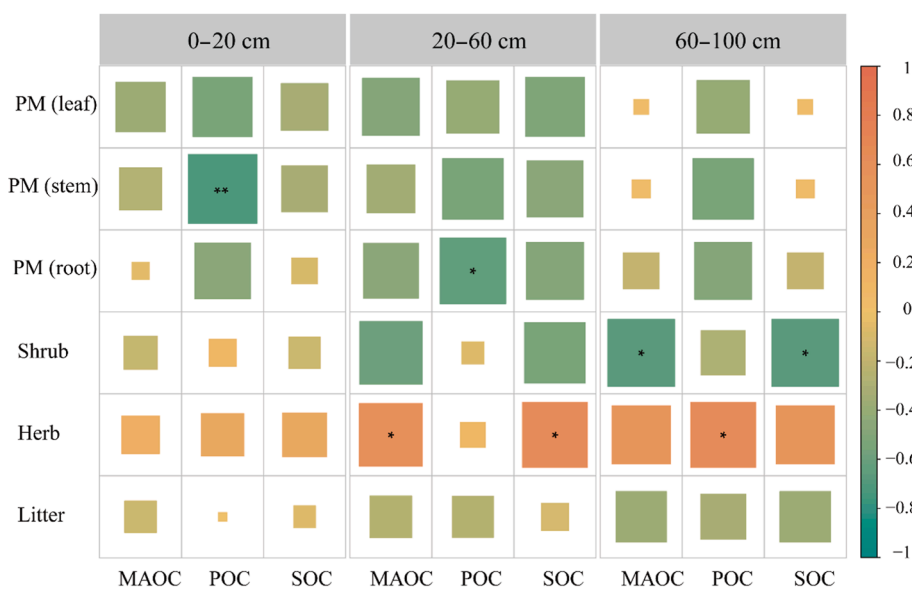


Fig. 5. Pearson correlation heatmap among SOC fractions content ($\text{g}\cdot\text{kg}^{-1}$), plant and litter carbon storage ($\text{t}\cdot\text{ha}^{-1}$) at different soil depths. Darker colors and larger shapes indicate stronger correlations. Significant correlations are marked with * $p < 0.05$ or ** $p < 0.01$.

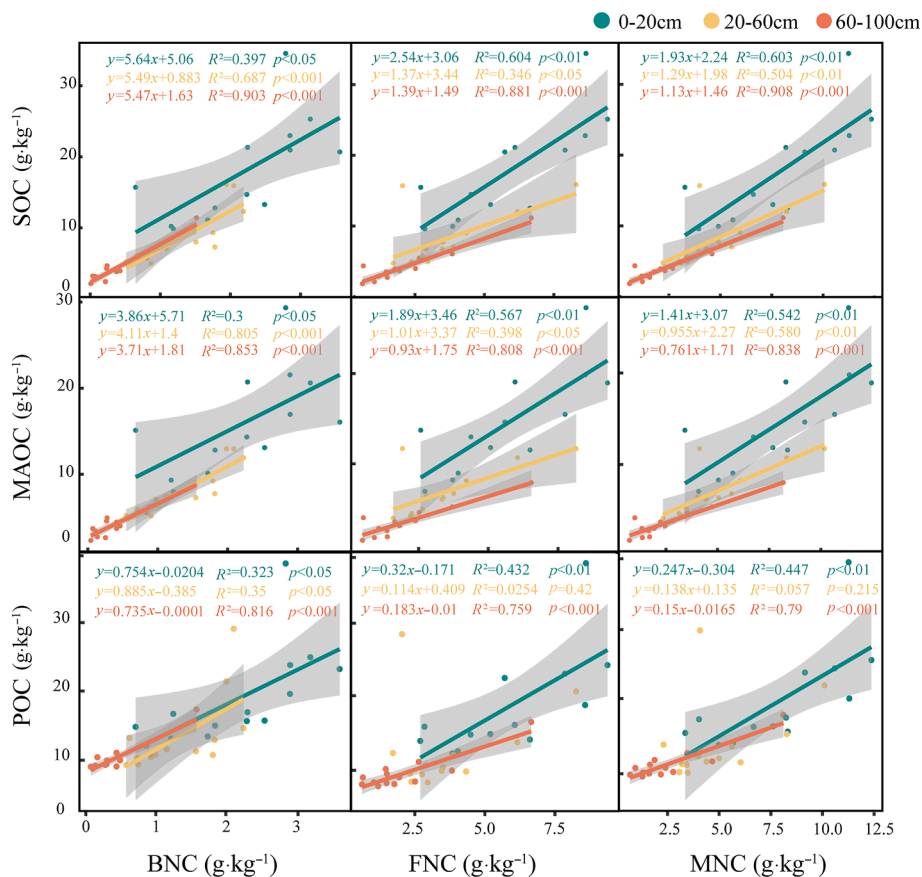


Fig. 6. Relationship between MNC and SOC fractions across soil depth as determined by linear regression analysis. The solid line denotes the fitted regression line, and the shaded band indicates the 95% confidence interval. Significant regression ($p < 0.05$) suggests a strong association.

4. Discussion

4.1. Ecosystem carbon storage remains stable across stand developmental stages

Total ecosystem C storage in *P. massoniana* reforestation did not vary significantly across stand developmental stages, reflecting different changes between plant and soil C pools (Fig. 1e). Plant C storage increased from 32 to 45 years due to larger DBH, but slightly declined thereafter as stand density decreased (Table S1). In contrast, SOC storage declined by 53.9% from 32 to 45 years and then recovered modestly at 60 years, mainly within the 0–60 cm layer (Fig. 1e). This contrasts with findings from Liu et al. (2025a), who reported increases of SOC across stand developmental stages likely arise from contrasting nutrient availability and mycorrhizal associations (Feng, 2022; Frey, 2019; Zhao et al., 2024). Specifically, soil available phosphorus (P) in our sites ranged only 1.12–1.56 mg·kg⁻¹ (Table S1), which were substantially lower than the values (1.60–1.94 mg·kg⁻¹) reported by Liu et al. (2025a). This low-P regime likely stimulates plants and microbes to accelerate soil organic matter decomposition to acquire P (Ding et al., 2021; Tie et al., 2024). On the other hand, *P. massoniana*, an ectomycorrhizal (ECM) species, produces slowly decomposing litter (Chae et al., 2019). This delays C transfer to the soil—a pattern consistent with the relatively high surface-layer SOC contents (approximately 23 g·kg⁻¹) than that (approximately 20 g·kg⁻¹) reported by Liu et al. (2025a), reflecting both C accumulation potential and slow turnover (Chae et al., 2019; Feng, 2022; Frey, 2019). In contrast, *Robinia pseudoacacia*, an arbuscular mycorrhizal (AM) species studied by Liu et al. (2025a), promotes faster carbon cycling (Frey, 2019; Liang et al.,

2017; Liu et al., 2025a), which aligns with its moderate yet synchronously increasing SOC levels.

Notably, the storage of POC declined more sharply than MAOC from 32 to 45 years (–68.4% vs. –49.0%), while MAOC storage recovery drove the SOC rebound from 45 to 60 years (+73.9%; Fig. 2c and d). The dynamics likely reflect a trade-off strategy between nutrient mining and mineral association (Ding et al., 2021; Hu et al., 2023; Tie et al., 2020). Our previous investigations conducted in these same experimental plots have demonstrated that P limitation becomes progressively more severe across stand developmental stages in *P. massoniana* plantations, characterized by a 65.2% decrease in labile P and a 59.7% reduction in moderately labile P between 32- and 60-year-old stands (Tie et al., 2024). Increasing P limitation across stand developmental stages (Tie et al., 2024) may stimulate nutrient mining (Ding et al., 2021; Frey, 2019), resulting in POC and MAOC losses during 32 to 45 years (Fig. 2c and d). Additionally, the increased understory vegetation diversity across stand developmental stages (Table S1) may have accelerated nutrient mining, further amplifying C loss during this stage (Li et al., 2026). However, the stronger soil P scarcity indicates increased soil mineral adsorption and protection, likely resulting in enhanced mineral sites and thus increased MAOC storage in the late stage of stand development (Lieberman et al., 2025; Spohn, 2024; Yi et al., 2023). The observed 78.6% increase in MNC (Figs. 4f) and 17.9% rise in acid phosphatase activity (Tie et al., 2024) between 45- and 60-years support this mechanism, indicating a shift to microbially and mineral mediated C stabilization in older stands.

4.2. SOC stability enhances along the chronosequence

The MAOC/POC ratio in the 0–100 cm soil layer increased 64.0% from 32 to 60 years (Fig. 3b), which may reflect a trend of enhanced SOC stability throughout stand development stages. This shift may be attributed to a more substantial reduction in POC storage (−68.4%) than in MAOC (−49.0%) between 32 and 45 years, and a recovery of MAOC (+73.9%) after 45 years (Fig. 2c and d). Because MAOC is physically and chemically protected by mineral surfaces, it resists decomposition, whereas POC represents more labile plant residues (Angst et al., 2023; Lavallee et al., 2019; Witzgall et al., 2021). Thus, the greater relative reduction in POC (−68.4%) between 32 and 45 years reflects intensified nutrient extraction and microbial decomposition (Ding et al., 2021; Frey, 2019), while the later MAOC increase likely corresponds to slightly enhanced microbial necromass formation (Fig. 4f–h) and mineral association (Adamczyk et al., 2019a; Angst et al., 2023; Ding et al., 2021; Reichert et al., 2022).

Additionally, we observed that the MAOC/POC ratio in the surface soil (0–20 cm) was lower compared to the subsoil (20–100 cm), although this difference was not statistically significant (Fig. 3a). This aligns with the “wedge concept” proposed by Hicks Pries et al. (2023), which posits that SOC in deeper layers is predominantly stable and accrues as a “wedge” over longtime scales due to differing stabilization mechanisms compared to surface soils. Indeed, surface soils, characterized by extensive rhizosphere and hyphosphere networks, exhibit a greater density of microbial activity hotspots (Kuzyakov and Blagodatskaya, 2015). However, subsoils experience reduced C inputs and diminished biological activity, making them more susceptible to mineralogical influences (Dubeux et al., 2024; Heinze et al., 2018; Hicks Pries et al., 2023). The stabilization of SOC in subsoils thus depends more on mineral properties (charge, surface area, Fe/Al oxides) than biological turnover (Dubeux et al., 2024; Heinze et al., 2018; Hicks Pries et al., 2023).

4.3. Microbial necromass dominates SOC, especially in deep soils

Microbial necromass accounted for approximately 50% of SOC in surface soils (0–20 cm) and up to 64.7% in subsoils (Fig. S3), exceeding the global forest averages of approximately 35% (Wang et al., 2021). The high Fe/Al oxide content typical of subtropical soils enhances mineral–organic associations, promoting microbial necromass retention (Sokol et al., 2018b; Tao et al., 2023; Yu et al., 2019). Consequently, microbial necromass is the primary contributor to SOC—especially MAOC—in these systems, whereas plant-derived inputs play a secondary role due to slow pine litter decomposition (Chae et al., 2019).

Positive correlations between SOC, MAOC, and microbial necromass (Fig. 6) further highlight the dominant microbial control on soil carbon. Interestingly, fungal necromass contributed more strongly than bacterial necromass (Fig. S3), and the FNC/BNC ratio closely tracked the MAOC/POC ratio (Fig. S4), indicating that fungal necromass may disproportionately support long-term SOC persistence. Notably, this enhanced contribution at least partly occurs even though absolute FNC storage did not increase significantly (Fig. 4), underscoring the high stabilization efficiency of fungal-derived C. This dominance of fungal necromass over bacterial necromass in the subsoil can be attributed to several interacting mechanisms (Adamczyk et al., 2019b; Strickland and Rousk, 2010; Su et al., 2023): (1) inherently more recalcitrant nature of fungal cell walls compared to bacterial cell structures; (2) higher carbon use efficiency (CUE) and elevated C/N ratios in fungi, resulting in greater residue production; and (3) enhanced stabilization of fungal necromass through complex interactions with tannins and other organic compounds. These findings position fungal necromass as a central mechanism underpinning SOC stability.

As soil depth increased, the slope of the relationship between microbial necromass and SOC fractions exhibited a decreasing trend (Fig. 6). This could be attributed to restricted microbial activity in the

subsoil environment (Dubeux et al., 2024; Hicks Pries et al., 2023). However, the R^2 values of correlations in the subsoil were relatively higher than those in surface soils (Fig. 6), indicating that microbial necromass likely explains a greater proportion of SOC dynamics in deep layers. This depth-dependent pattern can also support the microbial-centric perspective in deeper soils, which aligns with the understanding that subsoil carbon dynamics are increasingly governed by microbial processes and mineral associations (Hicks Pries et al., 2023).

Additionally, we observed weak correlations between plant/litter carbon storage and SOC fractions (Fig. 5). However, these weak correlations may not indicate a lack of ecological functional coupling, but likely reflect a temporal decoupling. Because plant and litter pools represent current or recent carbon inputs, whereas soil carbon pools—particularly MAOC—integrate long-term processes of carbon transformation and stabilization (Cotrufo et al., 2013; Parton et al., 2007).

4.4. Limitations and broader implications

This study reveals that mature *P. massoniana* reforestations maintain unchanged total C storage while progressively enhancing SOC stability. However, several uncertainties remain. First, the specific microbial pathways mediating in vivo turnover and ex vivo modification processes that drive SOC storage and stability across stand developmental stages remain poorly understood. Therefore, future studies should integrate microbial CUE (Tao et al., 2023), metagenomics (Wani et al., 2025), and DNA-SIP (Pepe-Ranney et al., 2015) approaches to identify taxa and traits governing POC-MAOC turnover, particularly in subsoils (Fig. S3). Second, our findings offer novel insights into the dynamics of soil C stability and ecosystem C storage across plants, litter, and soil, and reveal a close association between microbial necromass and SOC. However, these findings are predominantly based on correlational relationships. Future research could elucidate the underlying mechanisms of our observed results by conducting controlled experiments (e.g., nutrient addition, litter input, and laboratory incubations) and employing isotopic tracer techniques (e.g., ^{13}C and ^{33}P) to further elucidate the underlying mechanisms. Third, thinning represents a widely implemented forest management practice in pine reforestation systems (Deng et al., 2020; Liu et al., 2024). Although this study considered the potential effects of thinning-induced changes in stand density on age effects, forest age and thinning history are confounded along this chronosequence and cannot be fully disentangled. Therefore, our study captures the integrated dynamics of stand development under a specific management history, rather than the pure effect of forest age per se. Nevertheless, the observed patterns still provide valuable insights into the carbon dynamics of managed mature pine forests—a common and representative forest type in South China. Future studies should further distinguish the individual effects of stand density (or thinning) from those of stand age.

5. Conclusions

Our findings reveal a mechanistic transition in mature *P. massoniana* reforestations, where total ecosystem carbon storage remained relatively constant, while soil carbon stability may have increased substantially, reflected in a 64.0% rise in the 0–100 cm MAOC/POC ratio from 32 to 60 years. Microbial necromass constituted over half (45.9%–64.8%) of SOC, especially in the subsoils (20–100 cm), with fungal necromass dominating bacterial necromass. Hence, the ecosystem carbon persistence of pine mature reforestations derives not from additional carbon storage, but at least partly likely from the stability of SOC. Finally, integrating microbial necromass dynamics and subsoil stabilization processes into carbon models and forest management frameworks will improve predictions of pine reforestation's long-term role in carbon sequestration.

CRedit authorship contribution statement

Shiyang Wu: Writing – review & editing, Writing – original draft, Methodology, Formal analysis. **Liehua Tie:** Writing – review & editing, Writing – original draft, Formal analysis, Conceptualization. **Jordi Sardans:** Writing – review & editing, Writing – original draft. **Xingliang Xu:** Writing – review & editing, Writing – original draft. **Ji Chen:** Writing – review & editing, Writing – original draft. **Peilei Hu:** Writing – review & editing, Writing – original draft. **Lei Deng:** Writing – review & editing, Writing – original draft. **Yixian Kong:** Writing – original draft, Methodology, Formal analysis. **Shengnan Ouyang:** Writing – review & editing, Writing – original draft. **Congde Huang:** Writing – review & editing, Writing – original draft, Conceptualization. **Josep Peñuelas:** Writing – review & editing, Writing – original draft. **Guijie Ding:** Writing – review & editing, Writing – original draft.

Funding

This work was supported by the National Natural Science Foundation of China (Nos. 32460379 and 32360259), Guizhou Provincial Basic Research Program (ZK[2025]ZHONGDIAN070, ZK[2022]YIBAN101, and ZK[2023]YIBAN110), and Natural Science Project of Guizhou University [202131]. Josep Peñuelas and Jordi Sardans are financially supported by the Spanish Government grants PID2022-140808NB-I00 and PID2023-153125NB-I00 funded by the MICIU/AEI/10.13039/501100011033 and FEDER, EU.

Data availability

Data are available on request from the corresponding author.

Declaration of competing interest

The authors declare that they have no known competing financial interests or personal relationships that could have appeared to influence the work reported in this paper.

Appendix A. Supplementary data

Supplementary data to this article can be found online at <https://doi.org/10.1016/j.fecs.2026.100457>.

References

- Adamczyk, B., Sietiö, O.-M., Straková, P., Prommer, J., Wild, B., Hagner, M., Pihlatie, M., Fritze, H., Richter, A., Heinonsalo, J., 2019a. Plant roots increase both decomposition and stable organic matter formation in boreal forest soil. *Nat. Commun.* 10, 3982. <https://doi.org/10.1038/s41467-019-11993-1>.
- Adamczyk, B., Sietiö, O.-M., Biasi, C., Heinonsalo, J., 2019b. Interaction between tannins and fungal necromass stabilizes fungal residues in boreal forest soils. *New Phytol.* 223, 16–21. <https://doi.org/10.1111/nph.15729>.
- Angst, G., Mueller, K.E., Castellano, M.J., Vogel, C., Wiesmeier, M., Mueller, C.W., 2023. Unlocking complex soil systems as carbon sinks: multi-pool management as the key. *Nat. Commun.* 14, 2967. <https://doi.org/10.1038/s41467-023-38700-5>.
- Bai, Y., Zhou, Y., Chen, X., An, Z., Zhang, X., Du, J., Chang, S.X., 2023. Tree species composition alters the decomposition of mixed litter and the associated microbial community composition and function in subtropical plantations in China. *For. Ecol. Manag.* 529, 120743. <https://doi.org/10.1016/j.foreco.2022.120743>.
- Bai, Y., Zhou, Y., He, H., 2020. Effects of rehabilitation through afforestation on soil aggregate stability and aggregate-associated carbon after forest fires in subtropical China. *Geoderma* 376, 114548. <https://doi.org/10.1016/j.geoderma.2020.114548>.
- Bani, A., Pioli, S., Ventura, M., Panzacchi, P., Borruso, L., Tognetti, R., Tonon, G., Brusetti, L., 2018. The role of microbial community in the decomposition of leaf litter and deadwood. *Appl. Soil Ecol.* 126, 75–84. <https://doi.org/10.1016/j.apsoil.2018.02.017>.
- Bar-On, Y.M., Li, X., O'Sullivan, M., Wigneron, J.-P., Sitch, S., Ciaia, P., Frankenberg, C., Fischer, W.W., 2025. Recent gains in global terrestrial carbon stocks are mostly stored in nonliving pools. *Science* 387, 1291–1295. <https://doi.org/10.1126/science.adk1637>.
- Bossio, D.A., Cook-Patton, S.C., Ellis, P.W., Fargione, J., Sanderman, J., Smith, P., Wood, S., Zomer, R.J., von Unger, M., Emmer, I.M., Griscorn, B.W., 2020. The role of

- soil carbon in natural climate solutions. *Nat. Sustain.* 3, 391–398. <https://doi.org/10.1038/s41893-020-0491-z>.
- Brookes, P.C., Landman, A., Pruden, G., Jenkinson, D.S., 1985. Chloroform fumigation and the release of soil nitrogen: a rapid direct extraction method to measure microbial biomass nitrogen in soil. *Soil Biol. Biochem.* 17, 837–842. [https://doi.org/10.1016/0038-0717\(85\)90144](https://doi.org/10.1016/0038-0717(85)90144).
- Camenzind, T., Mason-Jones, K., Mansour, I., 2023. Formation of necromass-derived soil organic carbon determined by microbial death pathways. *Nat. Geosci.* 16, 115–122. <https://doi.org/10.1038/s41561-022-01100-3>.
- Cao, Q., Zhou, Y., Bai, Y., Han, Z., 2024. Available nitrogen and enzyme activity in rhizosphere soil dominate the changes in fine-root nutrient foraging strategies during plantation development. *Geoderma* 446, 116901. <https://doi.org/10.1016/j.geoderma.2024.116901>.
- Chae, H.M., Choi, S.H., Lee, S.H., Cha, S., Yang, K.C., Shim, J.K., 2019. Effect of litter quality on needle decomposition for four pine species in Korea. *Forests* 10, 371. <https://doi.org/10.3390/f10050371>.
- Cotrufo, M.F., Ranalli, M.G., Haddix, M.L., Six, J., Lugato, E., 2019. Soil carbon storage informed by particulate and mineral-associated organic matter. *Nat. Geosci.* 12, 989–994. <https://doi.org/10.1038/s41561-019-0484-6>.
- Cotrufo, M.F., Wallenstein, M.D., Boot, C.M., Deneff, K., Paul, E., 2013. The Microbial Efficiency-Matrix Stabilization (MEMS) framework integrates plant litter decomposition with soil organic matter stabilization: do labile plant inputs form stable soil organic matter? *Glob. Change Biol.* 19, 988–995. <https://doi.org/10.1111/gcb.12113>.
- Deng, C., Zhang, S., Lu, Y., Froese, R.E., Xu, X., Zeng, J., Ming, A., Liu, X., Xie, Y., Li, Q., 2020. Thinning effects on forest evolution in masson pine (*Pinus massoniana* Lamb.) conversion from pure plantations into mixed forests. *For. Ecol. Manag.* 477, 118503. <https://doi.org/10.1016/j.foreco.2020.118503>.
- Ding, W., Cong, W.-F., Lambers, H., 2021. Plant phosphorus-acquisition and -use strategies affect soil carbon cycling. *Trends Ecol. Evol.* 36, 899–906. <https://doi.org/10.1016/j.tree.2021.06.005>.
- Dou, X., Deng, Q., Li, M., Wang, W., Zhang, Q., Cheng, X., 2013. Reforestation of *Pinus massoniana* alters soil organic carbon and nitrogen dynamics in eroded soil in south China. *Ecol. Eng.* 52, 154–160. <https://doi.org/10.1016/j.ecoleng.2012.12.099>.
- Dubeux, J.C.B., Lira Junior, M.d.A., Simili, F.F., Bretas, I.L., Trumpp, K.R., Bizzuti, B.E., Garcia, L., Oduor, K.T., Queiroz, L.M.D., Acuña, J.P., Mendes, C.T.E., 2024. Deep soil organic carbon: a review. *CABI Rev.* 19, 24. <https://doi.org/10.1079/cabreviews.2024.0024>.
- FAO, 2020. Global Forest Resources Assessment 2020 – Key Findings. FAO, Rome, p. 16. <https://doi.org/10.4060/ca8753en>.
- Feng, X., 2022. Plant influences on soil organic carbon dynamics. In: Rumpel, C. (Ed.), *Understanding and Fostering Soil Carbon Sequestration. Burleigh Dodds Series in Agricultural Science*, Cambridge, UK, pp. 47–82.
- Frey, S.D., 2019. Mycorrhizal fungi as mediators of soil organic matter dynamics. *Annu. Rev. Ecol. Syst.* 50, 237–259. <https://doi.org/10.1146/annurev-ecolsys-110617-062331>.
- Gao, Y., Zhang, J., Tang, X., Wang, W., Yin, G., 2016. Variation of biomass and species richness in subtropical forest based on *Pinus massoniana* succession. *Ecol. Environ. Sci.* 25, 22–29. <https://doi.org/10.16258/j.cnki.1674-5906.2016.01.004>.
- Grimm, R., Behrens, T., Märker, M., Elsenbeer, H., 2008. Soil organic carbon concentrations and stocks on Barro Colorado Island — digital soil mapping using random forests analysis. *Geoderma* 146, 102–113. <https://doi.org/10.1016/j.geoderma.2008.05.008>.
- Griscorn, B.W., Adams, J., Ellis, P.W., Houghton, R.A., Lomax, G., Miteva, D.A., Schlesinger, W.H., Shoch, D., Siikamäki, J.V., Smith, P., Woodbury, P., Zganjar, C., Blackman, A., Campari, J., Conant, R.T., Delgado, C., Elias, P., Gopalakrishna, T., Hamsik, M.R., Herrero, M., Kiesecker, J., Landis, E., Laestadius, L., Leavitt, S.M., Minnemeyer, S., Polasky, S., Potapov, P., Putz, F.E., Sanderman, J., Silvius, M., Wollenberg, E., Fargione, J., 2017. Natural climate solutions. *Proc. Natl. Acad. Sci. USA* 114, 11645–11650. <https://doi.org/10.1073/pnas.1710465114>.
- Güner, Ş.T., Kiracioğlu, Ö., Sarimehmetoğlu, A., 2024. Changes in carbon stocks according to stand development stages in oriental beech forests in the Marmara Region of Türkiye. *Environ. Monit. Assess.* 196, 571. <https://doi.org/10.1007/s10661-024-12727-7>.
- Guo, Q., Li, H., Sun, X., An, Z., Ding, G., 2023. Patterns of needle nutrient resorption and ecological stoichiometry homeostasis along a chronosequence of *Pinus massoniana* plantations. *Forests* 14, 607. <https://doi.org/10.3390/f14030607>.
- He, J., Dai, Q., Xu, F., Yan, Y., Peng, X., 2021. Variability in soil macronutrient stocks across a chronosequence of masson pine plantations. *Forests* 13, 17. <https://doi.org/10.3390/f13010017>.
- Heinze, S., Ludwig, B., Piepho, H.-P., Mikutta, R., Don, A., Wordell-Dietrich, P., Helfrich, M., Hertel, D., Leuschner, C., Kirfel, K., Kandelner, E., Preusser, S., Guggenberger, G., Leinemann, T., Marschner, B., 2018. Factors controlling the variability of organic matter in the top- and subsoil of a sandy dystric cambisol under beech forest. *Geoderma* 311, 37–44. <https://doi.org/10.1016/j.geoderma.2017.09.028>.
- Hicks Pries, C.E., Ryals, R., Zhu, B., Min, K., Cooper, A., Goldsmith, S., Pett-Ridge, J., Torn, M., Berhe, A.A., 2023. The deep soil organic carbon response to global change. *Annu. Rev. Ecol. Syst.* 54, 375–401. <https://doi.org/10.1146/annurev-ecolsys-102320-085332>.
- Hu, H., Qian, C., Xue, K., Jörgensen, R.G., Keiluweit, M., Liang, C., Zhu, X., Chen, J., Sun, Y., Ni, H., Ding, J., Huang, W., Mao, J., Tan, R.-X., Zhou, J., Crowther, T.W., Zhou, Z.-H., Zhang, J., Liang, Y., 2024. Reducing the uncertainty in estimating soil microbial-derived carbon storage. *Proc. Natl. Acad. Sci. USA* 121, e2401916121. <https://doi.org/10.1073/pnas.2401916121>.

- Hu, J., Du, M., Chen, J., Tie, L., Zhou, S., Buckeridge, K.M., Cornelissen, J.H.C., Huang, C., Kuzyakov, Y., 2023. Microbial necromass under global change and implications for soil organic matter. *Glob. Change Biol.* 29, 3503–3515. <https://doi.org/10.1111/gcb.16676>.
- Hua, F.Y., Bruijnzeel, L.A., Meli, P., Martin, P.A., Zhang, J., Nakagawa, S., Miao, X.R., Wang, W.Y., McEvoy, C., Peña-Arancibia, J.L., Brancalion, P.H.S., Smith, P., Edwards, D.P., Balmford, A., 2022. The biodiversity and ecosystem service contributions and trade-offs of forest restoration approaches. *Science* 376, 839–844. <https://doi.org/10.1126/science.abl4649>.
- Joergensen, R.G., 2018. Amino sugars as specific indices for fungal and bacterial residues in soil. *Biol. Fertil. Soils* 54, 559–568. <https://doi.org/10.1007/s00374-018-1288-3>.
- Justine, M.F., Yang, W., Wu, F., Khan, M.N., 2017. Dynamics of biomass and carbon sequestration across a chronosequence of masson pine plantations. *J. Geophys. Res. Biogeosci.* 122, 578–591. <https://doi.org/10.1002/2016jg003619>.
- Kallenbach, C.M., Frey, S.D., Grandy, A.S., 2016. Direct evidence for microbial-derived soil organic matter formation and its ecophysiological controls. *Nat. Commun.* 7, 13630. <https://doi.org/10.1038/ncomms13630>.
- Kuzyakov, Y., Blagodatskaya, E., 2015. Microbial hotspots and hot moments in soil: concept & review. *Soil Biol. Biochem.* 83, 184–199. <https://doi.org/10.1016/j.soilbio.2015.01.025>.
- Lavallee, J.M., Soong, J.L., Cotrufo, M.F., 2019. Conceptualizing soil organic matter into particulate and mineral-associated forms to address global change in the 21st century. *Glob. Change Biol.* 26, 261–273. <https://doi.org/10.1111/gcb.14859>.
- Li, X., Ramos Aguila, L.C., Wu, D., Lie, Z., Xu, W., Tang, X., Liu, J., 2023. Carbon sequestration and storage capacity of Chinese fir at different stand ages. *Sci. Total Environ.* 904, 166962. <https://doi.org/10.1016/j.scitotenv.2023.166962>.
- Li, Y., Wu, J., Liu, Q., Yuan, J., Liu, F., Yuan, H., Mason-Jones, K., Li, Y., Lu, J., Peng, S., Li, Y., Ge, T., 2026. Priming effect on plant-derived mineral-associated organic C in paddy soil: a three-source partitioning study with a dual-¹³C approach. *Soil Biol. Biochem.* 214, 110073. <https://doi.org/10.1016/j.soilbio.2025.110073>.
- Liang, C., Schimel, J.P., Jastrow, J.D., 2017. The importance of anabolism in microbial control over soil carbon storage. *Nat. Microbiol.* 2, 17105. <https://doi.org/10.1038/nmicrobiol.2017.105>.
- Lieberman, H.P., von Sperber, C., Kallenbach, C.M., 2025. Soil phosphorus dynamics are an overlooked but dominant control on mineral-associated organic matter. *Glob. Change Biol.* 31, e70307. <https://doi.org/10.1111/gcb.70307>.
- Liu, C., Wang, B., Liu, J., Guo, C., Li, H., Zhang, H., Hu, Y., Ao, D., Xue, Z., An, S., Zhu, Z., 2025a. Arbuscular mycorrhizal fungi hyphal density rather than diversity stimulates microbial necromass accumulation after long-term *Robinia pseudoacacia* plantations. *Soil Biol. Biochem.* 206, 109817. <https://doi.org/10.1016/j.soilbio.2025.109817>.
- Liu, F., Liu, X., Zeng, M., Li, J., Tan, C., 2024. Thinning effects on aboveground biomass increments in both the overstory and understorey of masson pine forests. *Forests* 15, 1080. <https://doi.org/10.3390/f15071080>.
- Liu, M., Zheng, S., Pendall, E., Smith, P., Liu, J., Li, J., Fang, C., Li, B., Nie, M., 2025b. Unprotected carbon dominates decadal soil carbon increase. *Nat. Commun.* 16, 2008. <https://doi.org/10.1038/s41467-025-57354-z>.
- Minasny, B., Malone, B.P., McBratney, A.B., Angers, D.A., Arrouays, D., Chambers, A., Chaplot, V., Chen, Z.-S., Cheng, K., Das, B.S., Field, D.J., Gimona, A., Hedley, C.B., Hong, S.Y., Mandal, B., Marchant, B.P., Martin, M., McConkey, B.G., Mulder, V.L., O'Rourke, S., Richer-de-Forges, A.C., Odeh, I., Padarian, J., Paustian, K., Pan, G., Poggio, L., Savin, I., Stolbov, V., Stockmann, U., Sulaeman, Y., Tsui, C.-C., Vågen, T.-G., van Wesemael, B., Winowicki, L., 2017. Soil carbon 4 C per mille. *Geoderma* 292, 59–86. <https://doi.org/10.1016/j.geoderma.2017.01.002>.
- Návar, J., 2009. Allometric equations for tree species and carbon stocks for forests of northwestern Mexico. *For. Ecol. Manag.* 257, 427–434. <https://doi.org/10.1016/j.foreco.2008.09.028>.
- Nuralykyz, B., Nurzhan, A., Li, N., Huang, Q., Zhu, Z., An, S., 2023. Influence of land use types on soil carbon fractions in the Qaidam Basin of the Qinghai-Tibet Plateau. *Catena* 231, 107273. <https://doi.org/10.1016/j.catena.2023.107273>.
- Parton, W., Silver, W.L., Burke, I.C., Grassens, L., Harmon, M.E., Currie, W.S., King, J.Y., Adair, E.C., Brandt, L.A., Hart, S.C., Fasth, B., 2007. Global-scale similarities in nitrogen release patterns during long-term decomposition. *Science* 315, 361–364. <https://doi.org/10.1126/science.1134853>.
- Pepe-Ranney, C., Campbell, A.N., Koechli, C., Berthrong, S., Buckley, D.H., 2015. Unearthing the microbial ecology of soil carbon cycling with DNA-SIP. *bioRxiv*, 022483. <https://doi.org/10.1101/022483>.
- Prescott, C.E., 2010. Litter decomposition: what controls it and how can we alter it to sequester more carbon in forest soils? *Biogeochemistry* 101, 133–149. <https://doi.org/10.1007/s10533-010-9439-0>.
- Pugh, T.A.M., Lindeskog, M., Smith, B., Poulter, B., Arneeth, A., Haverd, V., Calle, L., 2019. Role of forest regrowth in global carbon sink dynamics. *Proc. Natl. Acad. Sci. USA* 116, 4382–4387. <https://doi.org/10.1073/pnas.1810512116>.
- Reichert, T., Rammig, A., Fuchslueger, L., Lugli, L.F., Quesada, C.A., Fleischer, K., 2022. Plant phosphorus-use and -acquisition strategies in Amazonia. *New Phytol.* 234, 1126–1143. <https://doi.org/10.1111/nph.17985>.
- Reinsch, S., Lebron, I., de Jonge, L.W., Weber, P.L., Norgaard, T., Arthur, E., Gomes, L., Pesch, C., Konstantinos, K., Zalidis, G., Epelde, L., Romic, M., Romic, D., Zovko, M., Reljic, M., Heikkinen, J., Feeney, C., Bentley, L., Levy, P., Vanguelova, E., Panagos, P., Schneider, F., Ahrens, B., Leifeld, J., Hugelius, G., Emmett, B.A., Cosby, B.J., Brentegani, M., Tandy, S., Thomas, A., van Soest, M.A.J., Robinson, D. A., 2025. The fraction of carbon in soil organic matter as a national-scale soil process indicator. *Glob. Change Biol.* 31, e70572. <https://doi.org/10.1111/gcb.70572>.
- Shan, R., Peng, G., Lin, Y., Ma, Z., 2025. Temporal stability of forest productivity declines over stand age at multiple spatial scales. *Nat. Commun.* 16, 2745. <https://doi.org/10.1038/s41467-025-57984-3>.
- Shang, R., Chen, J.M., Xu, M., Lin, X., Li, P., Yu, G., He, N., Xu, L., Gong, P., Liu, L., Liu, H., Jiao, W., 2023. China's current forest age structure will lead to weakened carbon sinks in the near future. *Innovation* 4, 100515. <https://doi.org/10.1016/j.xinn.2023.100515>.
- Shen, Y., Lei, L., Xiao, W., Cheng, R., Liu, C., Liu, X., Lin, H., Zeng, L., 2023. Soil microbial residue characteristics in *Pinus massoniana* lamb. Plantations. *Environ. Res.* 231, 116081. <https://doi.org/10.1016/j.envres.2023.116081>.
- Sokol, N.W., Kuebbing, S.E., Karlsen-Ayala, E., Bradford, M.A., 2018a. Evidence for the primacy of living root inputs, not root or shoot litter, in forming soil organic carbon. *New Phytol.* 221, 233–246. <https://doi.org/10.1111/nph.15361>.
- Sokol, N.W., Sanderman, J., Bradford, M.A., 2018b. Pathways of mineral-associated soil organic matter formation: integrating the role of plant carbon source, chemistry, and point of entry. *Glob. Change Biol.* 25, 12–24. <https://doi.org/10.1111/gcb.14482>.
- Spohn, M., 2024. Preferential adsorption of nitrogen- and phosphorus-containing organic compounds to minerals in soils: a review. *Soil Biol. Biochem.* 194, 109428. <https://doi.org/10.1016/j.soilbio.2024.109428>.
- Strickland, M.S., Rousk, J., 2010. Considering fungal:bacterial dominance in soils – methods, controls, and ecosystem implications. *Soil Biol. Biochem.* 42, 1385–1395. <https://doi.org/10.1016/j.soilbio.2010.05.007>.
- Su, Z., Zhong, Y., Zhu, X., Wu, Y., Shen, Z., Shanguan, Z., 2023. Vegetation restoration altered the soil organic carbon composition and favoured its stability in a *Robinia pseudoacacia* plantation. *Sci. Total Environ.* 899, 165665. <https://doi.org/10.1016/j.scitotenv.2023.165665>.
- Tang, J., Luysaert, S., Richardson, A.D., Kutsch, W., Janssens, I.A., 2014. Steeper declines in forest photosynthesis than respiration explain age-driven decreases in forest growth. *Proc. Natl. Acad. Sci. USA* 111, 8856–8860. <https://doi.org/10.1073/pnas.1320761111>.
- Tao, F., Huang, Y., Hungate, B.A., Manzoni, S., Frey, S.D., Schmidt, M.W.I., Reichstein, M., Carvalhais, N., Ciais, P., Jiang, L., Lehmann, J., Wang, Y.-P., Houlton, B.Z., Ahrens, B., Mishra, U., Hugelius, G., Hocking, T.D., Lu, X., Shi, Z., Viatkin, K., Vargas, R., Yigini, Y., Omuto, C., Malik, A.A., Peralta, G., Cuevas-Corona, R., Di Paolo, L.E., Luotto, I., Liao, C., Liang, Y.-S., Saynes, V.S., Huang, X., Luo, Y., 2023. Microbial carbon use efficiency promotes global soil carbon storage. *Nature* 618, 981–985. <https://doi.org/10.1038/s41586-023-06042-3>.
- Tie, L., Peñuelas, J., Huang, C., Sardans, J., Bose, A.K., Ouyang, S., Kong, Y., Guo, Y., Wu, Y., Cheng, W., Ding, G., 2024. Phosphorus limitation of *Pinus massoniana* reforestation increases with stand development: evidence from plant, leaf litter, and soil. *Plant Soil* 504, 817–832. <https://doi.org/10.1007/s11104-024-06661-3>.
- Tie, L., Zhang, S., Peñuelas, J., Sardans, J., Zhou, S., Hu, J., Huang, C., 2020. Responses of soil C, N, and P stoichiometric ratios to N and S additions in a subtropical evergreen broad-leaved forest. *Geoderma* 379, 114633. <https://doi.org/10.1016/j.geoderma.2020.114633>.
- Walkley, A., Black, I.A., 1934. An examination of the degtjareff method for determining soil organic matter, and a proposed modification of the chromic acid titration method. *Soil Sci.* 37, 29–38. <https://doi.org/10.1097/00010694-193401000-00003>.
- Wang, B., An, S., Liang, C., Liu, Y., Kuzyakov, Y., 2021. Microbial necromass as the source of soil organic carbon in global ecosystems. *Soil Biol. Biochem.* 162, 108422. <https://doi.org/10.1016/j.soilbio.2021.108422>.
- Wani, A.K., Qadir, F., Elboughdiri, N., Rahayu, F., Saefudin, Pranowo, D., Martasari, C., Kosmiatin, M., Suhara, C., Sudaryono, T., Prayogo, Y., Yadav, K.K., Muzammil, K., Eltayeb, L.B., Alreshidi, M.A., Singh, R., 2025. Metagenomics and plant-microbe symbioses: microbial community dynamics, functional roles in carbon sequestration, nitrogen transformation, sulfur and phosphorus mobilization for sustainable soil health. *Biotechnol. Adv.* 82, 108580. <https://doi.org/10.1016/j.biotechadv.2025.108580>.
- Witzgall, K., Vidal, A., Schubert, D.I., Höschen, C., Schweizer, S.A., Buegger, F., Pouteau, V., Chenu, C., Mueller, C.W., 2021. Particulate organic matter as a functional soil component for persistent soil organic carbon. *Nat. Commun.* 12, 4115. <https://doi.org/10.1038/s41467-021-24192-8>.
- WRB, I.W.G., 2015. *World Reference Base for Soil Resources 2014. International Soil Classification System for Naming Soils and Creating Legends for Soil Maps - Update 2015 (World Soil Resources Reports No. 106)*. FAO, Rome.
- Xiang, Y., Pan, P., Ouyang, X., Zang, H., Rao, J., 2020. The chemical stoichiometry characteristics of plant-soil carbon and nitrogen in subtropical *Pinus massoniana* natural forests. *Sci. Rep.* 14, 5031. <https://doi.org/10.1038/s41598-024-55740-z>.
- Xu, H., He, B., Guo, L., Yan, X., Zeng, Y., Yuan, W., Zhong, Z., Tang, R., Yang, Y., Liu, H., Chen, Y., 2024. Global forest plantations mapping and biomass carbon estimation. *J. Geophys. Res. Biogeosci.* 129. <https://doi.org/10.1029/2023JG007441>.
- Xu, J., Tian, H., Xiao, J., Li, Z., Xiao, W., Yin, R., 2025. Effects of close-to-nature forest management on carbon stocks in *Pinus tabulaeformis* plantations in northern China. *Front. For. Glob. Change* 7, 1495771. <https://doi.org/10.3389/ffgc.2024.1495771>.
- Xu, T., Chen, X., Hou, Y., Zhu, B., 2020. Changes in microbial biomass, community composition and diversity, and functioning with soil depth in two alpine ecosystems on the Tibetan Plateau. *Plant Soil* 459, 137–153. <https://doi.org/10.1007/s11104-020-04712-z>.
- Yi, C., Zhu, J., Chen, L., Huang, X., Wu, R., Zhang, H., Dai, X., Liang, J., 2023. Speciation of iron and aluminum in relation to phosphorus sorption and supply characteristics of soil aggregates in subtropical forests. *Forests* 14, 1804. <https://doi.org/10.3390/f14091804>.
- Yost, J.L., Hartemink, A.E., 2020. How deep is the soil studied – an analysis of four soil science journals. *Plant Soil* 452, 5–18. <https://doi.org/10.1007/s11104-020-04550-z>.
- Yu, M., Wang, Y., Jiang, J., Wang, C., Zhou, G., Yan, J., 2019. Soil organic carbon stabilization in the three subtropical forests: importance of clay and metal oxides.

- J. Geophys. Res. Biogeosci. 124, 2976–2990. <https://doi.org/10.1029/2018jg004995>.
- Zeng, G., Wang, H., Wu, S., Li, J., Zhao, Z., Dynamic changes of soil organic carbon storage of *Pinus sylvestris* var. *mongolica* plantations at different ages in Saihanba area. J. Sustain. For. 44, 1003–1016. <http://doi.org/10.1080/10549811.2025.2554861>.
- Zhang, K., Gao, D., Guo, H., Zeng, J., Liu, X., 2022a. Forest structure characteristics on soil carbon and nitrogen storage of *Pinus massoniana* plantations in southern subtropical region. Front. For. Glob. Change 5, 1022221. <https://doi.org/10.3389/ffgc.2022.1022221>.
- Zhang, Y., Zeng, D.-H., Lei, Z., Li, X., Lin, G., 2022b. Microbial properties determine dynamics of topsoil organic carbon stocks and fractions along an age-sequence of Mongolian pine plantations. Plant Soil 483, 441–457. <https://doi.org/10.1007/s11104-022-05757-y>.
- Zhao, G., Tariq, A., Zhang, Z., Nazim, M., Graciano, C., Sardans, J., Dong, X., Gao, Y., Peñuelas, J., Zeng, F., 2024. Afforestation with xerophytic shrubs promoted soil organic carbon stability in a hyper-arid environment of desert. Land Degrad. Dev. 36, 655–667. <https://doi.org/10.1002/ldr.5387>.
- Zhou, G., Liu, S., Li, Z., Zhang, D., Tang, X., Zhou, C., Yan, J., Mo, J., 2006. Old-growth forests can accumulate carbon in soils. Science 314. <https://doi.org/10.1126/science.1130168>, 1417–1417.
- Zhou, X., Wen, Y., Goodale, U.M., Zuo, H., Zhu, H., Li, X., You, Y., Yan, L., Su, Y., Huang, X., 2017. Optimal rotation length for carbon sequestration in *Eucalyptus* plantations in subtropical China. New For. 48, 609–627. <https://doi.org/10.1007/s11056-017-9588-2>.
- Zhu, J., Hu, H., Tao, S., Chi, X., Li, P., Jiang, L., Ji, C., Zhu, J., Tang, Z., Pan, Y., Birdsey, R.A., He, X., Fang, J., 2017. Carbon stocks and changes of dead organic matter in China's forests. Nat. Commun. 8, 151. <https://doi.org/10.1038/s41467-017-00207-1>.